

Hyperfine dependent gf -values of Mn I lines in the 1.49 – 1.80 μm H-band

M. Andersson^{1,2}, J. Grumer³, N. Ryde⁴, R. Blackwell-Whitehead⁴, R. Hutton^{1,2,6}, Y. Zou^{1,2},
P. Jönsson⁵ and T. Brage³

ABSTRACT

The three Mn I lines at 17325, 17339 and 17349 Å are among the 25 strongest lines ($\log(gf) > 0.5$) in the H-band. They are all heavily broadened due to hyperfine structure and the profiles of these lines have so far not been understood. Earlier studies of these lines even suggested that they were blended. In this work, the profiles of these three infra-red (IR) lines have been studied theoretically and compared to experimental spectra to assist in the complete understanding of the solar spectrum in the IR. It is shown that the structure of these lines can not be described in the conventional way by the diagonal A and B hyperfine interaction constants. The off-diagonal hyperfine interaction not only has large impact on the energies of the hyperfine levels, but also introduces a large intensity redistribution among the hyperfine lines, changing the line profiles dramatically. By performing large-scale calculations of the diagonal and off-diagonal hyperfine interaction and gf -values between the upper and lower hyperfine levels and using a semi-empirical fitting procedure, agreement between our synthetic and experimental spectra was achieved. Furthermore, we compare our results with observations of stellar spectra. The spectra of the Sun and the K1.5 III red giant star Arcturus were modelled in the relevant region, 1.73 – 1.74 μm using our theoretically predicted gf -values and energies for each individual hyperfine line. Satisfactory fits were obtained and clear improvements were found using our new data compared with the old available Mn I data. A complete list of energies and gf -values for all the $3d^5 4s(7S)4d e^6D - 3d^5 4s(7S)4f w^6F$ hyperfine lines are available as supplementary material online, whereas only the stronger lines are presented and discussed in detail in this paper.

Subject headings: atomic data, infrared: stars, line: identification, methods: laboratory: atomic, methods: numerical, stars: abundances

¹The Key lab of Applied Ion Beam Physics, Ministry of Education, China

²Shanghai EBIT laboratory, Modern physics institute, Fudan University, Shanghai, China

³Division of Mathematical Physics, Department of Physics, Lund University, Sweden

⁴Department of Astronomy, Lund University, Sweden

⁵School of Technology, Malmö University, Sweden

⁶Author to whom any correspondence should be addressed (e-mail: rhutton@fudan.edu.cn)

1. Introduction

High wavelength resolution spectrographs on satellite borne and ground based telescopes can resolve many of the absorption features in stellar spectra. In particular, line broadening effects such as hyperfine structure (HFS) and isotope shifts can be observed in the spectra of the Sun (Livingston & Wallace (1991)) and other stars (e.g. Arcturus, Hinkle et al. (1995a)). HFS increases the line width and decreases the peak intensity of the line profile. Omitting such effects will introduce an error in the measurement of the wavelength and the derived abundance from a stellar spectrum (Prochaska & McWilliam (2000)). It was shown by Jomaron *et al.* (1999), that if the HFS is not taken into account, the abundance of manganese in HgMn stars can be overestimated by up to three orders of magnitude. It was also shown that if the HFS of manganese is included as a crude estimate, the derived abundance may still be up to 4 times too large. Jomaron *et al.* (1999) suggested that the lack of accurate information about the HFS structure is the largest contributing factor to the uncertainty when estimating the abundance of manganese.

Hyperfine splitting of Mn I line profiles can be observed in the visible (Abt (1952)) and infrared (Swensson (1966)) spectrum of the Sun. In particular, Meléndez (1999) used the hyperfine split solar line profiles of Mn I in the H–band (1.49 to 1.80 μm) and J–band (1.00 to 1.34 μm) to measure the wavelength of the hyperfine component lines for the study of metal–rich stars in the Galactic bulge. However, Meléndez (1999) notes that the strong ($\log(gf) > -0.5$) Mn I lines at 17325, 17339 and 17349 Å have broad hyperfine splitting and appear to be blended with unknown features in the solar spectrum. Fitting these profiles is particularly difficult because there are no hyperfine structure constants in the literature for the upper levels ($3d^54s(^7S)4f\ w^6F_J$) of these transitions. Furthermore, the fine structure energy level values for w^6F_J are poorly known and the NIST atomic level database (Ralchenko *et al.* 2008) provides values from the work of Catalan et al. (1964) who used the Landé interval rule to calculate the energy level values from blended transitions in the UV. The high uncertainty in the energy level values for w^6F_J increases the uncertainty in the line identification and thus the fitting of the blended infra-red (IR) transitions. The laboratory line list for Mn I transitions in the IR by Taklif (1990) includes wavelengths for the 17325, 17339 and 17349 Å lines but Meléndez (1999) misinterprets the Taklif (1990) line list and identifies the 17325 Å feature as only the $3d^54s(^7S)4d\ e^6D_{9/2} - 3d^54s(^7S)4f\ w^6F_{9/2}$ transition. However, Taklif (1990) identifies the 17325 Å line as a blend of three transitions $e^6D_{9/2} - w^6F_{9/2}$, $e^6D_{9/2} - w^6F_{7/2}$ and $e^6D_{9/2} - w^6F_{11/2}$. A similar misinterpretation is given by Meléndez (1999) for the 17339 and 17349 Å features, which are reported by Taklif (1990) to be the following blended lines; $e^6D_{7/2} - w^6F_{9/2,7/2,5/2}$ (17339 Å) and $e^6D_{5/2} - w^6F_{7/2,5/2,3/2}$ (17349 Å).

A high resolution study of the spectrum of neutral manganese from the IR to the vacuum UV was reported in the thesis by Blackwell-Whitehead (2003) and further studies of the hyperfine structure are given in Blackwell-Whitehead *et al.* (2005). It was noted in Blackwell-Whitehead (2003) that it was not possible to fit the transitions from the w^6F term using diagonal hyperfine interaction constants. In this work Blackwell-Whitehead also indicated that the hyperfine splitting of the blended 17325, 17339 and 17349 Å lines may require a more detailed theoretical analysis to

fully understand these line profiles. Furthermore, given that 17325, 17339 and 17349 Å lines are within the 25 strongest ($\log(gf) > -0.5$) Mn I lines in the H-band, a study of their profiles will assist in the complete interpretation of the solar spectrum in the IR.

We show that the 17325, 17339 and 17349 Å line features are hyperfine split, blended features of the $e^6D_{9/2} - w^6F$, $e^6D_{7/2} - w^6F$ and $e^6D_{5/2} - w^6F$ transitions. These features can not be described using diagonal hyperfine interaction constants due to a strong off-diagonal hyperfine interaction which in some cases leads to such a large mixing between the hyperfine levels that the J -quantum number loses its meaning. Thus to assist in the analysis of these transitions in stellar spectra we provide individual, relative line positions and gf -values for each hyperfine transition. Furthermore, we suggest that the solar line profiles for 17325, 17339 and 17349 Å (air wavelengths) can be explained by off-diagonal hyperfine interaction and we claim that these lines are not significantly affected by unknown blends in the solar spectrum. These lines should therefore be useful in the analysis of stellar spectra, for instance in the determination of stellar Mn abundances.

2. Hyperfine interaction

In isotopes with a non-zero nuclear spin, I , there is an interaction between the electromagnetic moments of the nucleus and the electrons, which is often referred to as the hyperfine interaction. This interaction couples the total electronic angular momentum J and the nuclear spin I , to a new total angular momentum F . As a consequence of this interaction, each fine structure level is split up into several closely spaced hyperfine levels. If the energy separations between the fine structure levels are large compared to the separations due to the hyperfine interaction, the energies of the hyperfine levels can be calculated using lowest order perturbation theory

$$E_{hpf}(\gamma JF) = E_{fs}(\gamma J) + \frac{1}{2}AK \quad (1)$$

$$+ B \frac{(3/4)K(K+1) - J(J+1)I(I+1)}{2I(2I-1)J(2J-1)},$$

where $E_{fs}(\gamma J)$ is the energy of the fine structure level,

$$K = F(F+1) - J(J+1) - I(I+1), \quad (2)$$

and A and B are the hyperfine interaction constants. The label γ denotes the quantum numbers required to identify the fine structure level.

Manganese has only one stable isotope with a nuclear spin of $I = 5/2$ and a strong nuclear magnetic dipole moment, $\mu_I = 3.4687$ nuclear magnetons, as well as a small electric quadrupole moment, $Q = 0.32$ barns (Lide (2003)), leading to a potentially strong hyperfine interaction. The open $4s$ shell in the $3d^54s(^7S)4f w^6F$ term gives rise to a strong hyperfine interaction. At the same time the fine structure of this term is very small, resulting in a strong off-diagonal hyperfine interaction, i.e. interaction between hyperfine levels derived from different fine structure levels described in the diagonal approximation using the A and B interaction constants.

In order to describe a system where the fine and hyperfine structure energy splitting is of the same order of magnitude one has to use higher orders of perturbation calculation or use a matrix formalism to take the off-diagonal hyperfine interaction into account. In this work we have used the latter approach. We will not describe the method in detail in this paper but refer to three earlier papers which were based on similar approaches, Andersson *et al.* (2006), Grumer *et al.* (2010) and Andersson *et al.* (2012).

To describe the hyperfine states we couple the J -dependent electronic wave function $|\gamma J\rangle$ to the nuclear wave function $|I\rangle$ using standard coupling theory to build F -dependent wave functions $|\gamma JIF\rangle$ (FSF) which form a set of basis functions in our calculation. The Atomic State Function (ASF), $|\Gamma F\rangle$, representing the hyperfine mixed hyperfine levels, is written as a linear combination of the FSFs as

$$|\Gamma F\rangle = \sum_i c_i |\gamma_i J_i I F\rangle, \quad (3)$$

where c_i are expansion coefficients.

In the calculation of the lower hyperfine levels all possible $|e^6D JIF\rangle$ and $|e^8D JIF\rangle$ FSFs were used and for the upper hyperfine levels all $|w^6F JIF\rangle$ and $|w^8F JIF\rangle$. Using these basis functions the hyperfine interaction Hamilton matrix was set up and diagonalized to yield hyperfine level energies and the expansion coefficients of the ASFs.

The transition operator acts only on the electronic part of the wave function and the nuclear part can therefore be decoupled. The gf -values of the hyperfine transitions can then be calculated in terms of J -dependent transition matrix elements as

$$\begin{aligned} gf &= \frac{8\pi^2 m_e c a_0^2 \sigma}{3h} (2F_i + 1)(2F_j + 1) \\ &\times \left| \sum_i \sum_j (-1)^{J_i} c_i c_j \right. \\ &\times \left. \left\{ \begin{array}{ccc} F_i & J_i & I \\ J_j & F_j & 1 \end{array} \right\} \langle \gamma_i J_i || \mathbf{D}^{(1)} || \gamma_j J_j \rangle \right|^2. \end{aligned} \quad (4)$$

For details, see Grumer *et al.* (2010).

3. Method of Calculation

The calculations were based on first optimizing wave functions for the lower e^6D_J and the upper w^6F_J fine structure levels using the relativistic atomic structure package GRASP2K (Jönsson *et al.* 2013). These programs are based on the multiconfiguration Dirac-Hartree-Fock (MCDHF) method as outlined by Grant (2007). The even and the odd states were optimized in two separate calculations. Using the electronic wave functions the Hamiltonian matrix, including the hyperfine interaction, was constructed and diagonalized using the HFSZEEMAN program (Andersson &

Jönsson (2008)) to give the hyperfine level energies as well as the corresponding wave functions in the form of equation (3).

Having the ASFs for the hyperfine levels, the gf -values of the transitions were calculated using a newly developed code, connected to the GRASP2K suite of programs, which determines rates of F -dependent transitions in a general manner (Grumer *et al.* (unpublished)). Note that this code also allows for an external magnetic field in cases when it is large enough to be non-negligible. The program is based on equation (4) and uses the mixing coefficients from HFSZEEMAN together with the J -dependent transition matrix elements from a slightly modified version of the GRASP2K transition program.

To investigate the importance of the off-diagonal hyperfine interaction, two different calculations were performed. The first we have named the *Complete* calculation and the second the *Diagonal* calculation. In the *Complete* calculation, the full hyperfine interaction matrix was used, whereas in the *Diagonal* calculation only the diagonal hyperfine interaction matrix elements were included. The *Diagonal* calculation therefore corresponds to describing the hyperfine interaction in terms of A and B hyperfine interaction constants.

4. Laboratory Measurements

The emission spectrum of manganese, fig 2 to 4, was recorded at the National Institute of Standards and Technology (NIST) with the NIST 2-m Fourier transform spectrometer (Nave *et al.* 1997) using resolutions of 0.008 to 0.03 cm^{-1} , which is sufficient to fully resolve the Doppler broadened line profiles of the transitions. The light-source used was a water-cooled hollow cathode lamp (Blackwell-Whitehead 2003; Blackwell-Whitehead *et al.* 2005). Owing to the brittle nature of pure manganese, the cathodes were made of an alloy of 95% Mn and 5% Cu. The hollow cathode was run at a current of 1.5 A, with 1.9 Torr of Ne as a buffer gas.

5. Synthetic spectra

The laboratory spectra were recorded using a hollow cathode, and the line intensities of a spectrum from such a light source should be proportional to the gf -values under the assumption that the transition rates are much higher than the collision rates and that line intensities from the same multiplet are compared. The synthetic spectra were generated by giving each hyperfine line a Voigt profile and the Full Width Half Maximum (FWHM) was fitted to the experimental spectrum.

To be able to reproduce the experimental spectrum it was necessary to adjust our *ab initio* energies. The energies of the e^6D levels have been determined experimentally but the fine structure of the w^6F term is poorly known. The NIST atomic level database (Ralchenko *et al.* 2008) provides values from the work of Catalan *et al.* (1964) who used the Landé interval rule to calculate the

energy level values from blended transitions in the UV. However, since the hyperfine interaction is of the same order as the fine structure splitting, this method should be considered invalid.

To start from accurate fine structure energies is of great importance since the hyperfine mixing is very sensitive to the fine structure splitting. The fine structure splitting of the w^6F levels is very small compared to the term splitting between w^6F and $3d^54s(^7S)4f\ z^8F$. Since the fine structure is associated with the spin-orbit interaction and this interaction is responsible for the mixing between the levels of w^6F and z^8F , the fine structure of w^6F should be close to the Landé interval rule,

$$E_{fs}(LSJ) = \frac{\mathcal{C}(LS)}{2}[J(J+1) - L(L+1) - S(S+1)] \quad (5)$$

where \mathcal{C} is the Landé interval constant. We used this argument as a start when trying to reproduce the experimental spectrum. By using the error defined by the least square fit between the synthetic and experimental spectra, the Landé interval constant was varied to find the best fit. The resulting value of \mathcal{C} was in this case found to be 0.0150 cm^{-1} . We will refer to results using this method as *Landé Fitted*.

To further improve the fitting and allow for deviations from the Landé interval rule, the energies of the independent fine structure levels were varied. This was also done by using the error defined by the least square fit between the synthetic and experimental spectra. Using this approach good agreement was found between the synthetic and experimental spectra. Results based on this model will be referred to as *Level Fitted*.

In general, even if theoretically predicted gf -values are close to experimental ones, the predicted energies for the lines are not of experimental accuracy. To improve our synthetic spectra we therefore made a final adjustment where we allowed for small variations of the hyperfine level energies when fitting to experimental spectra. In these adjustments, only the hyperfine level energies were changed, whereas all gf -values were kept fixed. We again used the error defined by the least square fit between the synthetic and experimental spectra to find a better fit. We allowed for variations for both the lower and upper hyperfine levels resulting in 54 free parameters. Our computer power was not large enough to handle so many parameters, but we had to try to improve the spectra stepwise, going from the upper to the lower end of the spectrum. Using this approach we could reproduce the experimental spectrum to very high accuracy. We will refer to results including this final adjustment as *Hyperfine Adjusted*.

6. Results and Discussion

Besides trying to reproduce the experimental spectra and obtaining information about all individual hyperfine lines, we also investigated the importance of the off-diagonal hyperfine interaction, and how important the different steps of our fitting procedure were to reproduce the experimental spectra. The influence of the off-diagonal hyperfine interaction can be found by comparing the results from *Diagonal* and *Complete* calculations (see section 3).

Using the *Landé Fitted* method, described in section 5, we performed *Diagonal* and *Complete* calculations trying to fit the synthetic spectra to experiment by varying the Landé interval constant. The former of these we will refer to as the *Diagonal* and the latter as *Complete Lande Fitted (CLaF)* calculation. Comparing the spectra from these two calculations, the importance of the off-diagonal hyperfine interaction can be found.

Including the off-diagonal hyperfine interaction we performed two further calculations, the *Complete Level Fitted (CLeF)* using the *Level Fitted* procedure described in section 5, and the *Complete Hyperfine Adjusted (CHA)* using the *Hyperfine Level Adjusted* method also described in section 5.

Comparing the synthetic spectra from the *CLaF* calculation to the one from the *CLeF* calculation, the influence of adjusting the fine structure energies of w^6F from the Landé interval rule can be determined. Finally, the impact of adjusting the individual hyperfine level energies to the synthetic spectra can be investigated by comparing the spectra from the *CLeF* calculation on the spectra from the *CHA* calculation.

To see how the synthetic spectra changed through the *Diagonal*, *CLaF*, *CLeF* and *CHA* calculations, we have chosen to present the 17339 Å spectral feature, corresponding to the $e^6D_{7/2}-w^6F$ hyperfine lines, for these four calculations in Figure 1. The differences between the four different synthetic spectra for the 17325, 17349, 17357 and 17362 Å spectral features, corresponding to the $e^6D_{9/2,5/2,3/2,1/2}-w^6F$ hyperfine lines, follows much the same pattern.

From Figure 1 it is found that the *Diagonal* calculation in principle predicts one strong peak surrounded on both sides with some weak structure. The spectrum from the *CLaF* calculation predicts a much wider and more complex structure and there are in principle no similarities between the two spectra. It should be pointed out that these differences are entirely due to the off-diagonal hyperfine interaction, which not only affects the energies of the hyperfine levels but also has a very large impact on the *gf*-values of the individual hyperfine transitions. It is clear from this picture that the hyperfine levels of w^6F can not be described in terms of *A* and *B* hyperfine constants.

Moving from the *CLaF* to the *CLeF* spectrum it is found that the position and the intensities of some lines have been slightly changed, but the differences are rather small. The same is found going from *CLeF* to *CHA*. It should be pointed out that going from *CLaF* to *CLeF* did not only change the position of the hyperfine lines but also slightly changed the *gf*-values, whereas going to *CHA* only changed the position of the hyperfine lines whereas the *gf*-values were the same as for *CLeF*.

Below we give some results in detail for the three spectral regions of e^6D-w^6F of greatest astrophysical interest. For each group of peaks we present a figure (Figure 2-4) where we have plotted our synthetic spectrum from the *CHA* calculation compared to the experimental one. In each figure we also present the synthetic spectrum from the *Diagonal* calculation as an inset plot.

The off-diagonal hyperfine interaction gives rise to many new transitions and the total number

of transitions within each sub-spectrum can therefore be very large, and the total transition list is therefore too long to be published in the paper version of this article but is available as online supplementary material. Instead we have chosen to present those lines that have a gf -value equal to or greater than 10% of the largest gf -value within each sub-spectrum. These lines give a good description of the spectrum and the additional lines only make small changes and the reduced list is therefore sufficient for discussing the results.

In each table, various information about each hyperfine line is presented. In the first column the F -value of the w^6F hyperfine level is given. The second column is labelled HFS, and refers to HyperFine State. This is an index identifying the different hyperfine levels in the calculations. Since the off-diagonal hyperfine interaction introduces a large mixing between the hyperfine states in this system, the J -value is no longer a good quantum number and can therefore not be used to identify the hyperfine levels. Instead we gave each hyperfine level an identification number according to the energy order of the hyperfine levels within each parity symmetry. In column three and four the corresponding information is given for e^6D hyperfine levels. In column five, the wavenumber from the *CHA* calculation for the hyperfine transition is given, and in the sixth column the gf value from the same calculation is given. In column seven the gf -value from the corresponding hyperfine transition in the *Diagonal* calculation is given and in the last column is the difference in gf -value of the *Diagonal* calculation relative to the *CHA* calculation. The complete $e^6D - w^6F$ line list can be found as supplementary material online.

The accuracy of the wavenumbers should undoubtedly be high as the atomic energy structure is deduced from high quality wavefunctions and subsequently anchored to high precision laboratory spectra. The values in the tables are therefore given with four decimals. The estimated uncertainties of the relative positions, which are the important quantities here, are smaller than $\pm 0.02 \text{ cm}^{-1}$. This is better than what is required for stellar spectroscopy. It should be made clear that uncertainties of the absolute wavenumbers are slightly higher as they are dependent on the calibration of the experimental spectra.

6.1. The 17325 Å line

We start by investigating the 17325 Å line corresponding to the $e^6D_{9/2} - w^6F$ transitions in the interval $5770.0 - 5770.6 \text{ cm}^{-1}$. The result is presented as a plot in Figure 2 and in detail in Table 1. From Figure 2 it is found that our *CHA* synthetic spectrum reproduces the features of the experimental one, whereas the *Diagonal* calculation predicts a structure that is too simple. The main differences between the *Diagonal* and the *CLeF* spectra are the two peaks emerging at 5770.30 cm^{-1} and 5770.33 cm^{-1} . From Table 1 it is found that the predicted gf -values for the hyperfine transitions making up these lines are about 25% smaller in the *Diagonal* calculation than in the *CLeF* calculation. The fact that these two lines emerge in the spectrum generated from the *CLeF* calculation is only partly explained by the enhancement of the gf -values. The main underlying reason is rather the shift in energy induced by the off-diagonal hyperfine interaction.

6.2. The 17339 Å line

The 17339 Å line is situated in the region $5765.3 - 5766.0 \text{ cm}^{-1}$. The comparison between the experimental and the *CHA* spectra is presented in Figure 3. In the same figure the spectrum from the *Diagonal* calculation is also included as an inset plot. Starting with the *Diagonal* spectrum it is found that it in principle predicts only one peak, whereas the experimental spectrum of the $e^6D_{7/2} - w^6F$ transitions is much more complex. The *CHA* synthetic spectrum on the other hand reproduces all features of the experimental one. The largest difference between *CHA* and experiment is the line at 5765.43 cm^{-1} . In *CHA* this peak is approximately 10% lower than experiment and it is positioned at an energy that is 0.007 cm^{-1} too low.

The results are presented in detail in Table 2. It is found that there are much larger differences between the *Diagonal* and *CLeF* calculation for this part of the spectrum than for the 17325 Å spectral feature. Even the *gf*-values for the strongest and second strongest lines differ by 10% and 28% respectively. Even more notable is that there are three lines in the list that have *gf*-values which are identically zero in the *Diagonal* calculation, and that the strongest of these have a *gf*-value which is 14% of the strongest of all lines in this part of the spectrum. It is clear from this list that the changes to the *gf*-values due to the off-diagonal hyperfine interaction have a very large impact on the spectrum.

6.3. The 17349 Å line

The 17349 Å line is situated in the region $5761.7 - 5762.6 \text{ cm}^{-1}$. In the main plot of Figure 4 we compare our *CHA* synthetic spectrum to the experimental. The corresponding spectrum generated from the *Diagonal* calculation is presented as an inset plot. Comparing the *Diagonal* synthetic spectrum to experiment it is found that it is far off the target and that there are not many similarities between the two spectra for the $e^6D_{5/2} - w^6F$ transitions. However, there is a good resemblance between the *CHA* synthetic spectrum and the experimental one.

Inspecting the results of the $e^6D_{5/2} - w^6F$ hyperfine transitions as presented in Table 3, it is found that the differences between the *CLeF* and *Diagonal* calculation are even larger than for the 173325 and 17339 Å spectral features in the spectrum. The transition with the largest *gf*-value differs by 36% between the two calculations and the 4th strongest line, with a *gf*-value of 42% of the largest, in the *CHA* calculation is a strictly forbidden transition in the *Diagonal* calculation. Actually, the 4th, 5th, 8th, 10th and 14th strongest lines of the 22 transitions in the line list are all induced by the off-diagonal hyperfine interaction and are absent in the *Diagonal* spectrum. This has of course a very large impact on the spectrum and is a further proof of the invalidity of describing the hyperfine structure of the $e^6D - w^6F$ spectrum in terms of A and B hyperfine constants.

6.4. Uncertainties of the gf -values

As it is hard to give any precise values of the *absolute* gf -uncertainties in the present work, we focus the current discussion on the *relative* uncertainties. These are undoubtedly also the most relevant quantities to discuss as the absolute values anyway are easy to rescale with an overall common factor, possibly evaluated from a comparison with a well-calibrated measurement. Nevertheless, even though there is little experience about hyperfine structure analyzes of a complexity comparable to the present work, we expect the overall uncertainty of the *absolute* gf -values to be well below 10%.

The uncertainty of the *relative* gf -values can be estimated from comparisons of the synthetic spectra to the corresponding experimental spectra as presented in Figures 2, 3 and 4. By investigating all hyperfine components of these spectra, one can conclude that the synthetic line which seems to fit worst with experiment is the left-most line of Figure 3 at 5765.43 cm^{-1} . This line has a gf -value which is about 10% too small as compared to experiment which was noted above in Section 6.2. It should however be clear that this is the worst case scenario as the synthetic spectrum could be scaled up with a factor to better fit this line with the spectrum and thereby instead overestimate the group of lines in the center of this part of the spectrum. One could therefore consider 10% as an upper limit of the relative gf -uncertainty. Furthermore it should be noted that this line is an example of a transition which is not at all predicted by a conventional A and B hyperfine constant (or *Diagonal*) analysis. Another line which doesn't fit perfectly with the experimental spectrum is the structure just right of the main peak in Figure 2 at 5770.25 cm^{-1} . The gf -value of this line deviates from experiment by approximately 5%. Apart from these two lines we judge the overall uncertainty of the *relative* gf -values to be well within 5%.

7. Modeling stellar Mn I lines

A way to test our new calculations of the hyperfine splitting of the Mn lines, is to compare with observations of stellar spectra. We have therefore modelled the spectra of the Sun (of spectral type G2V) and of the K1.5 III red giant star Arcturus (α Boo) in the relevant spectral region of $1.73 - 1.74 \mu\text{m}$ in order to be able to compare with the atlases of these stars by Livingston & Wallace (1991) and Hinkle et al. (1995a), respectively. The spectral resolution of these atlases is sufficiently high to resolve the stellar spectral lines. We calculated the synthetic spectra for atmospheres modelled with the MARCS code (Gustafsson *et al.* 2008)¹.

These model atmospheres are hydrostatic and are computed on the assumptions of Local Thermodynamic Equilibrium (LTE), chemical equilibrium, homogeneous plane-parallel (for the Sun) or spherically-symmetric (for Arcturus) stratification, and the conservation of the total flux

¹For the Sun we use $T_{\text{eff}} = 5770 \text{ K}$, $\log g = 4.44$, $\xi_{\text{micro}} = 0.93 \text{ km s}^{-1}$, and solar abundances, and for Arcturus $T_{\text{eff}} = 4280 \text{ K}$, $\log g = 1.7$, $\xi_{\text{micro}} = 1.74 \text{ km s}^{-1}$, $[\text{Fe}/\text{H}] = -0.53$, $[\alpha/\text{Fe}] = +0.30$, see Ryde *et al.* (2010) for details.

(radiative plus convective; the convective flux being computed using the local mixing length recipe).

The synthetic spectra were calculated in plane parallel and spherical symmetry for the Sun and Arcturus, respectively. We sample the spectra with a resolution of $R = 600,000$. With a micro-turbulence velocity of $1 - 2 \text{ km s}^{-1}$, this will ensure an adequate sampling. We finally convolve our synthetic spectra, in order to fit the shapes and widths of the observed lines, with a macro-turbulent (and instrumental) broadening, represented by a radial-tangential function Gray (1992), with 2.2 and 3.7 km s^{-1} (FWHM), respectively. The code used for calculating the synthetic spectra is BSYN v. 7.09 which is based on routines from the MARCS code. A $^{12}\text{C}/^{13}\text{C}$ ratio of 89 is used for the Sun, and of 9 for Arcturus, see e.g. Ryde *et al.* (2010).

The atomic line list used in our calculations is compiled from the VALD database (Piskunov *et al.* (1995)). When needed, we determined ‘astrophysical gf -values’ by fitting atomic lines in the synthetic spectra to the solar spectrum. The lines fitted were, among others, 8 Fe, 3 C, 1 Ca, and 2 Ti lines. In addition, the new strengths ($\log gf$) of the hfs Mn lines are calculated, but are given in a relative scale. The lines fit the best when we scale the strengths by a factor of 5. The molecular line lists, which include CO, OH, CN, SiO, CH, were adopted as they are and instead of modifying the gf values, the abundances of $\log \epsilon_{\text{O}} = 8.63$ (from OH lines), then $\log \epsilon_{\text{C}} = 8.06$ (from CO lines) and last $\log \epsilon_{\text{N}} = 7.67$ (from CN lines) were obtained from the Arcturus atlas, in good agreement with Ryde *et al.* (2009). For the Sun a $\log \epsilon_{\text{CNO}} = (8.41, 7.80, 8.66)$ abundance is assumed.

In Figure 5 we show our fits to the solar spectrum around the Mn lines by plotting the normalized flux versus frequency given by the wavenumber in cm^{-1} . In this region the very wide Brackett 10 hydrogen line ($n = 4 - 10$) dominates and complicates the comparison. Especially, the normalization of the flux spectrum in this region is difficult since the continuum is absent over a wide frequency range due to the hydrogen line. Furthermore, existing codes calculating the broadening and strengths of solar hydrogen lines cannot fit these lines. We have therefore manipulated the hydrogen opacity by artificially changing the $\log gf$ value for this line in order to fit the local ‘continuum’ when analyzing the Mn lines. The entire spectral region shown in Figure 5 is more or less affected by the hydrogen line. Thus, the original $\log gf = -0.417$ is changed to $\log gf = -0.55$, except for the H-core region, where for the low frequency side of the Ni line ($5756 - 5757 \text{ cm}^{-1}$), it is changed to $\log gf = -0.75$ and on the high side ($5759 - 5760 \text{ cm}^{-1}$), to $\log gf = -0.65$. The local synthetic spectra thus calculated are shown in the figure. We also show a synthetic spectrum with the original Mn line list (in blue) and compare this to the spectrum calculated with the new one (in red). The new fit is very satisfactory. The Mn lines at 5770 cm^{-1} ($17\,325 \text{ \AA}$) are, however, too strong in the synthetic spectrum compared to the observed spectrum, the reason of which is not understood.

In Figure 6 we present our synthetic fit to the observed spectrum of the cooler giant star Arcturus. We see directly the appearance of the many molecular lines from CO, CN, and OH, which dominate the spectrum. The hydrogen line is now more narrow, as expected for a lower gravity star, with less collisional broadening. The hydrogen line was fitted by changing the opacity

through a change in the $\log gf_{\text{HBA}10}$ to -0.7 . The general fit to the spectrum of this star is very good and especially the synthesized spectrum using the new data of the Mn lines (in red) is an improvement compared with the fit that was possible using previous data (in blue). Again, the Mn lines at 5770 cm^{-1} ($17\,325 \text{ \AA}$) are too strong in the synthesized spectrum, for reasons which require further investigations. We note however that these lines lie in the blue wing of a strong Si line, the broadening of which is not accurately synthesized.

As demonstrated in the figures of both the Sun and Arcturus, a few of the Mn lines are nearly absent in the spectra using the old data. For other Mn lines the residuals between the observed and synthesized spectra have more than halved when using the new data.

8. Conclusions

We have combined theoretical synthetic and experimental spectra of the $3d^5 4s(^7S)4d \text{ e}^6\text{D} - 3d^5 4s(^7S)4f \text{ w}^6\text{F}$ 17325, 17339, 17349, 17357 and 17362 \AA lines in Mn I to derive information about the individual hyperfine lines that make up these five spectral features. We have modelled the spectra of the sun and the red giant star Arcturus using the new atomic data as well as using previously published atomic data and we have shown that our new data generates a better fit to observed stellar spectra. Using the new hyperfine structure data, these lines should therefore be useful in the analysis of stellar spectra.

Due to the extensive number of hyperfine transitions in this system we have concentrated our discussion on the three strong groups of hyperfine transitions called the 17325, 17339 and 17349 \AA lines and only included the strongest of the transitions of each of these sub groups in the tables of this paper. A complete list of all the individual $\text{e}^6\text{D} - \text{w}^6\text{F}$ hyperfine transitions can be found as online material.

We have shown that the hyperfine levels involved in these transitions can not be described in terms of the conventional hyperfine constants. Instead they have to be described individually due to the large impact of the off-diagonal hyperfine interaction. By fitting our theoretical spectra to experimental ones by allowing for small adjustments to the calculated fine structure energies and hyperfine interaction matrix elements in an iterative procedure we think we have developed a method that could be applied to similar problems in other atomic and ionic systems of interest to the astrophysical community.

9. Acknowledgments

Dr. Paul Barklem is thanked for discussions concerning the modelling of the Hydrogen Ba 10 line and Dr. Kjell Eriksson for valuable help and discussions concerning the running of the MARCS model-atmosphere program.

M. Andersson is financed by the EU under the Science & Technology Fellowship Programme China (STF).

JG would like to thank the Nordic Centre at Fudan University, Shanghai, for supporting his visit to Fudan in 2013.

N. Ryde is a Royal Swedish Academy of Sciences Research Fellow supported by a grant from the Knut and Alice Wallenberg Foundation. N. Ryde also acknowledges support from the Swedish Research Council, VR, and Funds from Kungl. Fysiografiska Sällskapet i Lund.

EPSRC and PPARC of the UK supported the experimental studies undertaken by RWB while a PhD student at Imperial College London.

RH and YZ acknowledge the support of the National Natural Science Foundation of China under project no. 11074049 and by the Shanghai Leading Academic Discipline Project B107.

P. Jönsson and T. Brage acknowledges support from the Swedish research council.

REFERENCES

Abt, A. 1952, *Ap.J.*, 115, 199

Andersson, M., Jönsson, P., and Sabel, H., 2006, *J. Phys. B: At. Mol. Opt. Phys.*, 39, 4239

Andersson, M., and Jönsson, P., 2008, *Comput. Phys. Commun.*, 178, 156

Andersson, M., Lennartsson, T., Nilsson, H. Chen, C.Y., 2012, *J. Phys. B: At. Mol. Opt. Phys.*, 45, 135001

Blackwell-Whitehead, R.J. 2003, Ph.D. thesis, Imperial College, London

Blackwell-Whitehead, R., Pickering, J.C., Pearse, O., Nave, G. 2005, *Ap. J. S.*, 157, 402

Blackwell-Whitehead, R., Nilsson, H., Hartmann, H. 2009, *Opt. Soc. Am. Technical Digest (Optical Society of America, 2009)*, paper FTuA3

Blackwell-Whitehead, R., private communication.

Catalan, M.A., Meggers, W.F., and Garcia-Riquelme, O. 1964, *J. Res. Natl. Bur. Stand.* 68A, 9

Grant, I. P, 2007, *Relativistic Quantum Theory of Atoms and Molecules: Theory and Computation (Springer Series on Atomic, Optical and Plasma Physics, Berlin: Springer 2007)*

Gray, D. F., 1992, *The observation and analysis of stellar photospheres*, Cambridge ; New York : Cambridge University Press, 1992 2nd ed.

Grumer, J, Andersson, M, and Brage, T, 2010 *J. Phys. B: At. Mol. Opt. Phys.*, 43, 074012

- Grumer, J., Andersson, M. and Jönsson, P. (to be submitted to Comput. Phys. Comm. for publication)
- Gustafsson, B., Edvardsson, B., Eriksson, K., *et al.*, 2008, A&A 486, 951
- Hinkle, K., Wallace, L., and Livingston, W., 1995a, PASP107, 1042
- Hinkle, K., Wallace, L., Livingston, W. C. 1995b, Infrared atlas of the Arcturus spectrum, 0.9 - 5.3 microns (Astronomical Society of the Pacific Monograph Publications)
- Jomaron, C.M., Dworetzky, M.M., & Allen, C.S. 1999, MNRAS, 303, 555
- Jönsson, P., Gaigalas, .G, Bieroń, J., Froese Fischer, C., and Grant, I. P., 2013, Comput. Phys. Comm. 184, 2197
- Nave, G., Sansonetti, C. J., & Griesmann, U. 1997, Opt. Soc. Am. Tech. Digest Ser. 3, Fourier Transform Spectroscopy: Methods and Applications (Washington: Opt. Soc. Am.), 38
- Danzmann, K., Gunther, M., Fischer, J., Kock, M., & Kuhne, M. 1988, Appl. Opt., 27, 4947
- Learner, R.C.M., & Thorne, A.P. 1988, J. Opt. Soc. Am. B, 5:10, 2045
- Lide, D., ed CRC Handbook of Chemistry and Physics (84:th ed.; Boca Raton: CRC Press)
- Livingston, W., & Wallace, L. 1991, N.S.O. Tech. Rep., 91-001
- Meléndez, J. 1999, MNRAS, 307, 197
- Piskunov, N. E., Kupka, F., Ryabchikova , T. A., Weiss, W. W. and Jeffery, C. S., 1995, A&AS, 112, 525
- Prochaska J. X., McWilliam A., 2000, ApJ, 537, L57
- Ralchenko, Yu., Kramida, A.E., Reader, J. and NIST ASD Team 2008, NIST Atomic Spectra Database (version 3.1.5), [Online]. Available: <http://physics.nist.gov/asd3> [2010, February 17]. National Institute of Standards and Technology, Gaithersburg, MD
- Ryde, N., Edvardsson, B., Gustafsson, B., Eriksson, K., Käuffl, H. U., Siebenmorgen, R., and Smette, A., 2009, A&A, 496, 701
- Ryde, N., Gustafsson, B., Edvardsson, B., Meléndez, J., Alves-Brito, A., Asplund, M., Barbuy, B., Hill, V., Käuf, H. U., Minniti, D., Ortolani, S., Renzini, A., and Zoccali, M., 2010, A&A, 509, A20
- Swensson, J.W. 1966, Die Naturwissenschaften, 53, 330
- Taklif, A.G. 1990, Phys. Scr., 42, 69

Whaling, W., Anderson, W. H. C., Carle, M. T., Brault, J. W., Zarem, H. A. 1995, *J. Quant. Spec. Radiat. Trans.*, 53, 1

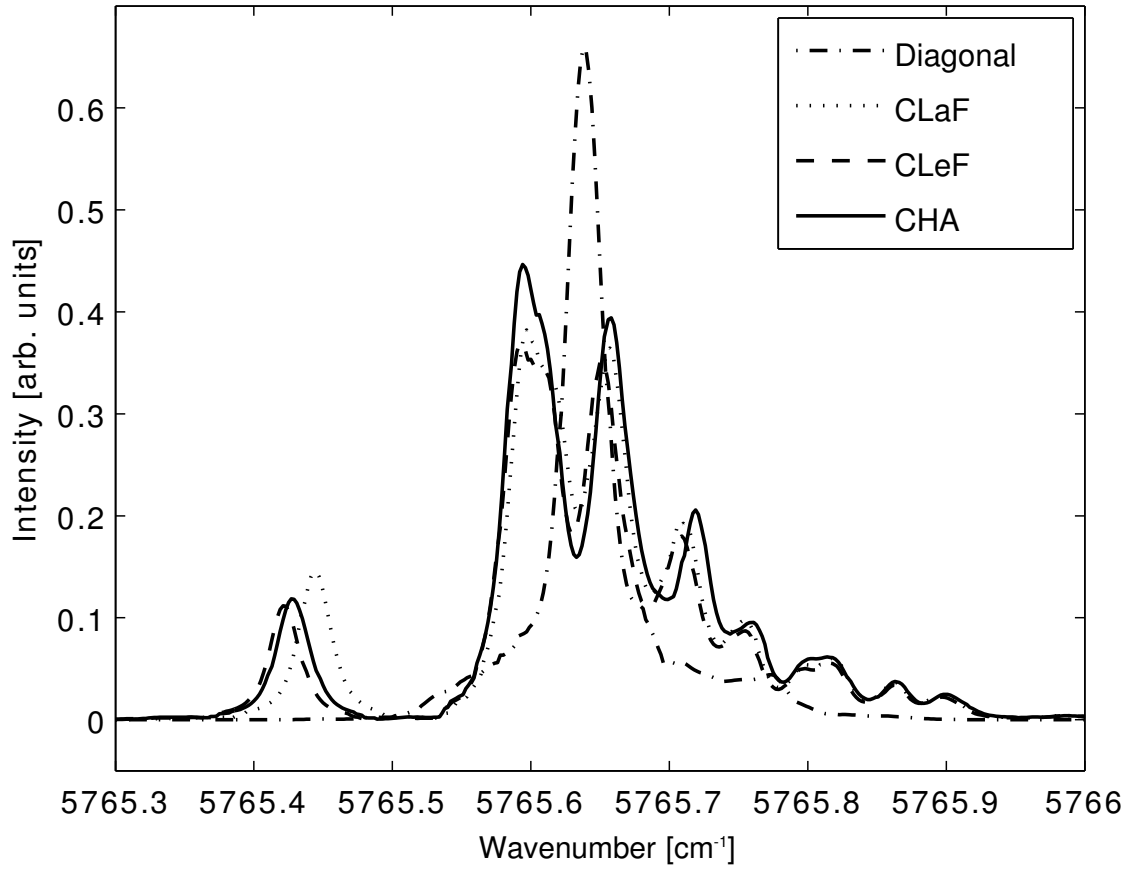


Fig. 1.— Four different synthetic spectra of the $e^6D_{7/2}-w^6F$ transitions (the 17339Å line). The dash-dotted spectrum is from the Diagonal calculation, the dotted from the Complete Lande Fitted calculation (CLaF), the dashed from the Complete Level Fitted (CLeF) and the solid from the Complete Hyperfine Level Adjusted (CHA).

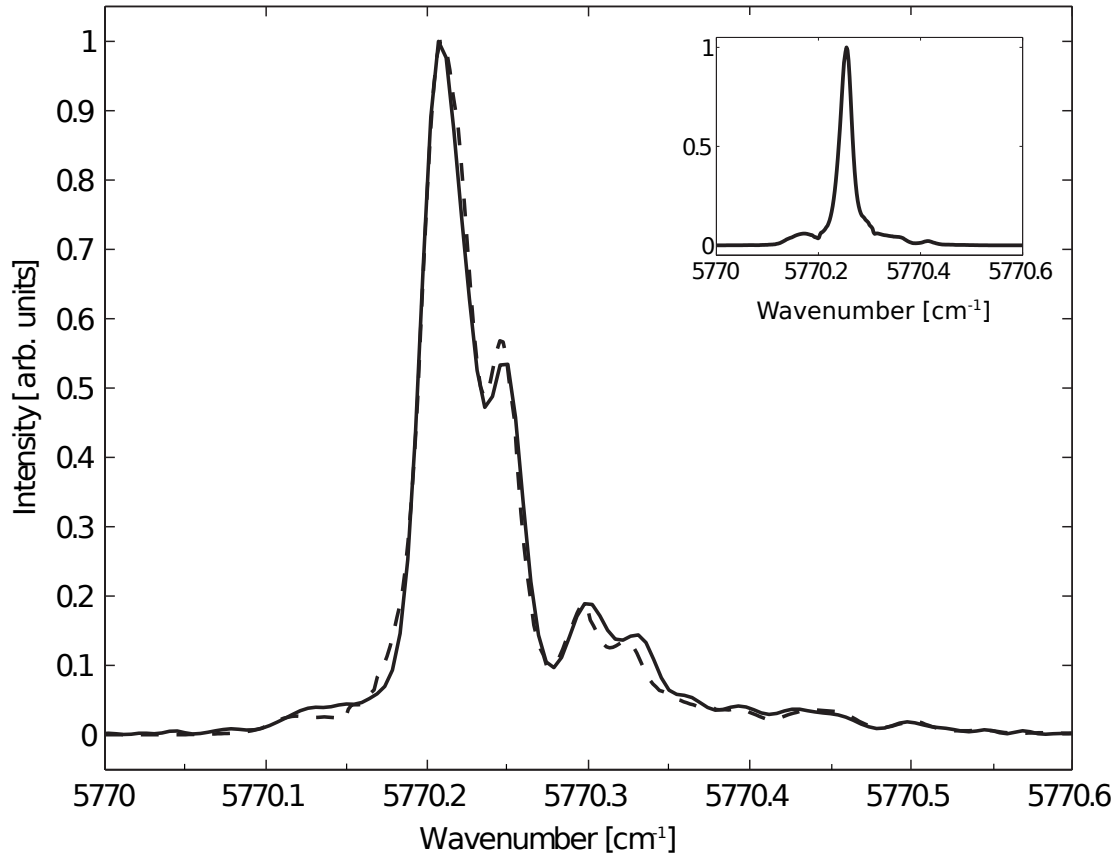


Fig. 2.— The experimental spectrum (solid line) compared to the *CHA* spectrum (dashed line) for the $e^6D_{9/2}-w^6F$ transitions (the 17325\AA line). The *Diagonal* spectrum is presented as an inset plot.

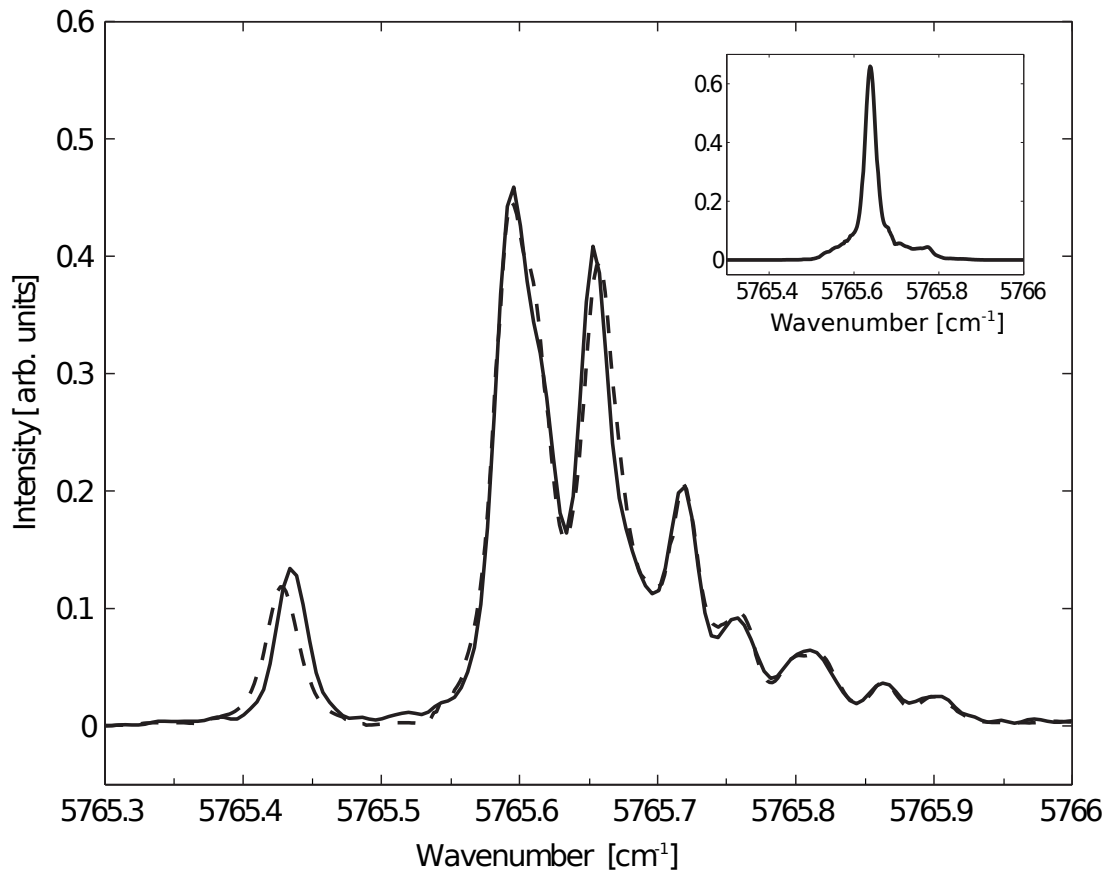


Fig. 3.— The experimental spectrum (solid line) compared to the *CHA* spectrum (dashed line) for the $e^6D_{7/2}-w^6F$ transitions (the 17339Å line). The *Diagonal* spectrum is presented as an inset plot.

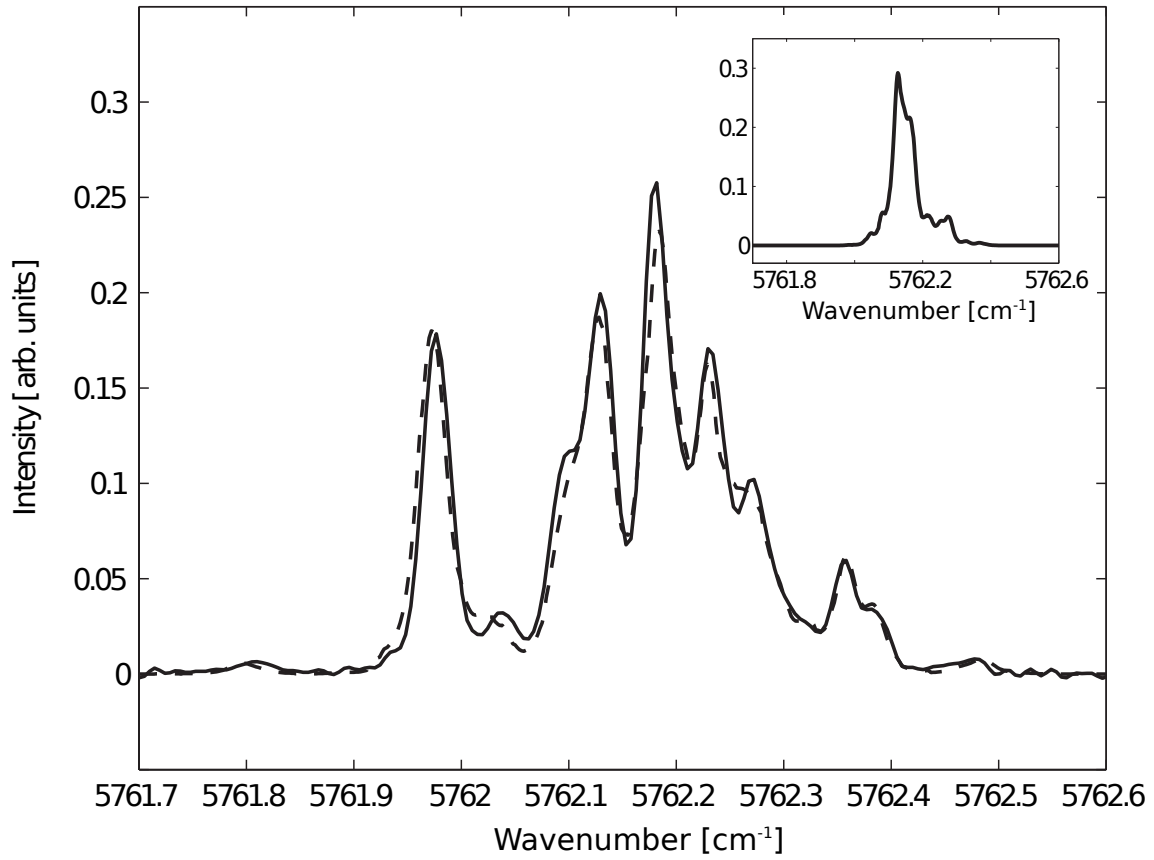


Fig. 4.— The experimental spectrum (solid line) compared to the *CHA* spectrum (dashed line) for the $e^6D_{5/2}-w^6F$ transitions (the 17349Å line). The *Diagonal* spectrum is presented as an inset plot.

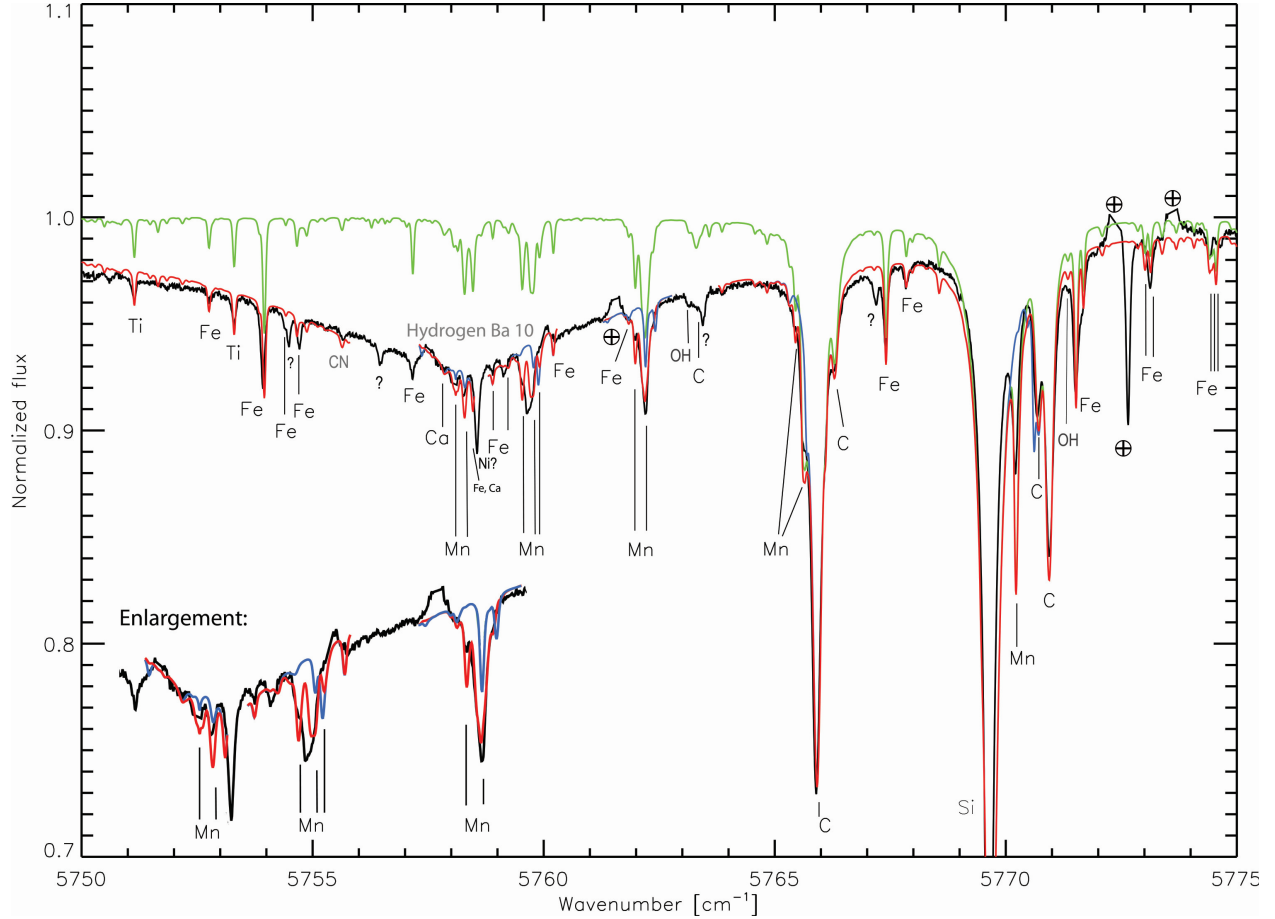


Fig. 5.— Section of the observed solar spectrum Livingston & Wallace (1991) is shown in black. Our best synthetic spectra are shown in red, and include our newly calculated Mn lines. In green we show the same spectrum, but omitting the Hydrogen Bracket 10 line, to show its influence. The blue spectrum shows the spectrum using the Mn line list from the VALD database. All synthetic lines which are deeper than 0.97 of the continuum are identified. A few features not identified are labelled with question marks. Regions where the elimination of strong telluric lines resulted in a degradation of the spectrum are marked with an Earth symbol. In the lower left corner an enlargement of the spectrum (not shown to scale) is plotted in order to show the fits in greater detail.

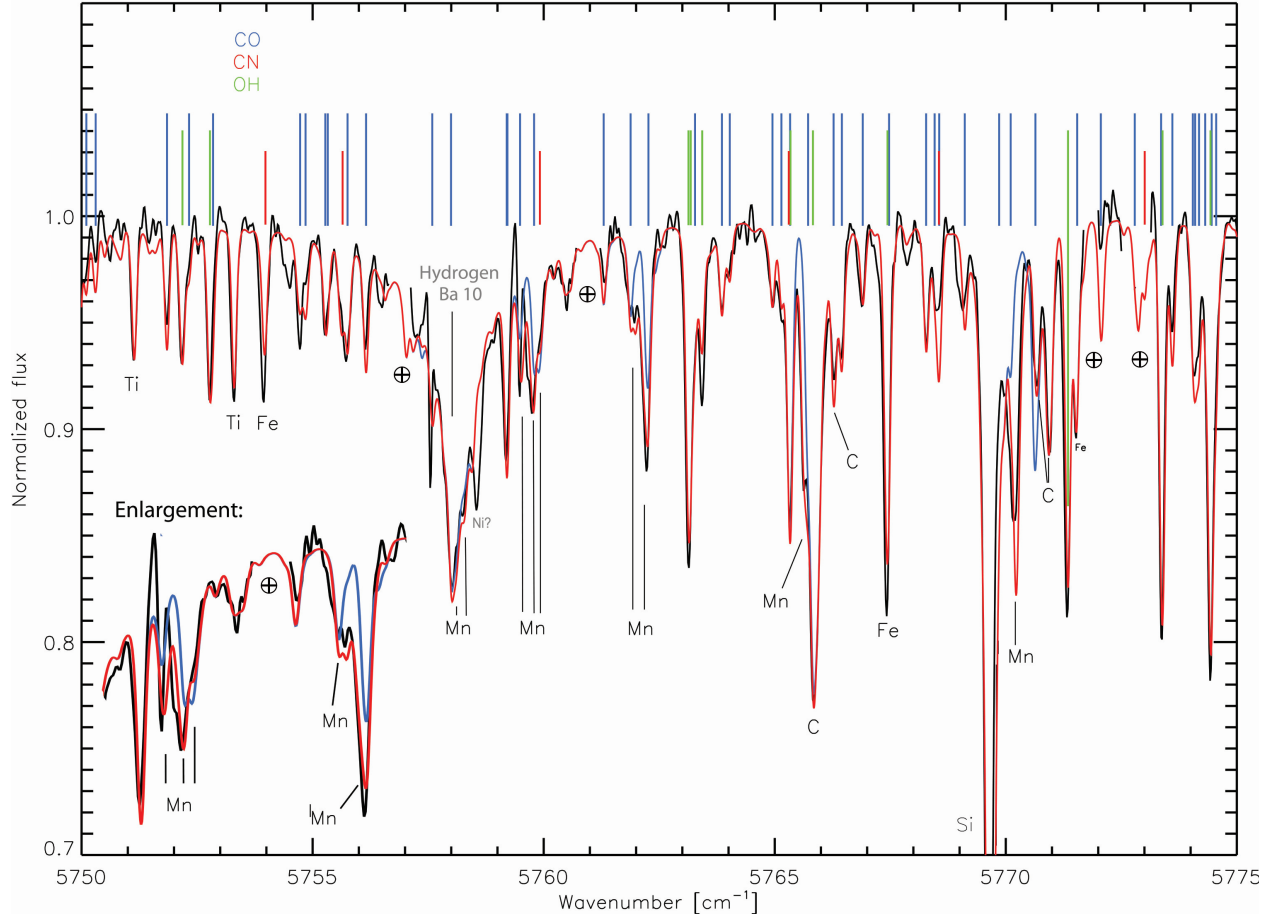


Fig. 6.— The wavelength region of interest for our newly calculated Mn lines is displayed. The observed spectrum of the K1.5 III giant *Arcturus* (Hinkle *et al.* (1995b)) is shown in black and our best synthetic spectrum is shown in red, which includes our newly calculated Mn lines. The blue spectrum shows the spectrum using the Mn line list from the VALD database. All synthetic lines which are deeper than 0.97 of the continuum are identified. Regions where the elimination of strong telluric lines resulted in a degradation of the spectrum are marked with an Earth symbol. In the lower left corner an enlargement of the spectrum (not shown to scale) is plotted in order to show the fits in greater detail.

Table 1. Line list of the $e^6D_{9/2}-w^6F$ transitions (the 17325 Å line) based on theoretical calculations. Only those with a gf -value of at least 10% of the largest gf -value have been included. HFS is a hyperfine level index. See Section 6 for discussions about the wavenumber and gf -value uncertainties.

w^6F		e^6D		Complete		Diagonal	Δgf (%)
F	HFS	F	HFS	Wavenumber (cm^{-1}) ^a	gf ^b	gf	
5	39	4	31	5770.2040	5.895	6.047	3
4	38	3	30	5770.2033	4.875	4.859	-0
3	37	2	29	5770.2047	3.999	3.916	-2
6	42	5	32	5770.2126	7.193	7.475	4
7	47	6	33	5770.2212	8.898	9.153	3
8	54	7	34	5770.2474	1.109×10^1	1.109×10^1	0
5	46	5	32	5770.2917	1.281	9.455×10^{-1}	-26
6	52	6	33	5770.2983	1.707	1.269	-26
7	61	7	34	5770.3259	2.219	1.692	-24

^a Our recommended wavenumbers with an estimated overall relative uncertainty less than 0.02 cm^{-1} .

^b Our recommended gf -values with an estimated overall uncertainty of 5%.

Table 2. Line list of the $e^6D_{7/2}-w^6F$ transitions (the 17339 Å line) based on theoretical calculations. Only those with gf -values of at least 10% of the largest gf -value have been included. HFS is a hyperfine level index. See Section 6 for discussions about the wavenumber and gf -value uncertainties.

w ⁶ F		e ⁶ D		Complete		Diagonal	Δgf (%)
F	HFS	F	HFS	Wavenumber (cm ⁻¹) ^a	gf ^b	gf	
5	39	4	38	5765.4221	8.493×10^{-1}	0	–
6	42	5	39	5765.4283	1.002	0	–
7	47	6	40	5765.4371	7.791×10^{-1}	0	–
3	41	2	36	5765.5891	2.563	2.704	5
4	43	3	37	5765.5901	2.884	3.650	27
5	46	4	38	5765.5943	3.574	4.831	35
2	40	1	35	5765.6043	2.212	1.991	-10
6	52	5	39	5765.6137	4.899	6.263	28
4	50	4	38	5765.6496	1.207	1.146	-5
7	61	6	40	5765.6579	7.160	7.964	11
5	56	5	39	5765.6728	1.967	1.753	-11
2	45	2	36	5765.6911	7.873×10^{-1}	4.918×10^{-1}	-38
6	64	6	40	5765.7191	3.196	2.595	-19
3	55	3	37	5765.7455	7.959×10^{-1}	6.942×10^{-2}	-91
5	56	4	38	5765.7597	8.283×10^{-1}	4.023×10^{-1}	-51
4	58	4	38	5765.7982	9.405×10^{-1}	6.545×10^{-2}	-93
5	65	5	39	5765.8638	7.462×10^{-1}	4.363×10^{-2}	-94

^a Our recommended wavenumbers with an estimated overall relative uncertainty less than 0.02 cm⁻¹.

^b Our recommended gf -values with an estimated overall uncertainty of 5%.

Table 3. Line list of the $e^6D_{5/2}$ - w^6F transitions (the 17349 Å line) based on theoretical calculations. Only those with a gf -value of at least 10% of the largest gf -value have been included. HFS is a hyperfine level index. See Section 6 for discussions about the wavenumber and gf -value uncertainties.

w^6F		e^6D		Complete		Diagonal	Δgf (%)
F	HFS	F	HFS	Wavenumber (cm^{-1}) ^a	gf ^b	gf	
5	46	4	45	5761.9605	1.632	0	–
4	43	3	44	5761.9661	1.428	0	–
6	52	5	46	5761.9707	1.265	0	–
3	41	2	43	5761.9790	8.594×10^{-1}	0	–
3	48	2	43	5762.0822	8.391×10^{-1}	1.720	105
4	50	3	44	5762.0904	1.217	2.627	116
2	45	1	42	5762.1138	1.319	1.032	-22
3	55	3	44	5762.1196	4.518×10^{-1}	6.925×10^{-1}	53
5	56	4	45	5762.1261	2.124	3.783	78
1	44	0	41	5762.1315	8.210×10^{-1}	5.350×10^{-1}	-35
4	58	4	45	5762.1431	1.309	1.484	13
6	64	5	46	5762.1700	3.845	5.216	36
3	55	2	43	5762.1840	7.301×10^{-1}	6.677×10^{-1}	-9
2	53	2	43	5762.1971	9.588×10^{-1}	2.473×10^{-1}	-74
5	65	5	46	5762.2039	3.043	2.720	-11
4	58	3	44	5762.2413	6.580×10^{-1}	6.595×10^{-1}	0
4	63	5	46	5762.2547	1.016	5.505×10^{-1}	-46
3	57	3	44	5762.2582	1.126	0	–
2	60	3	44	5762.2783	6.592×10^{-1}	1.802×10^{-1}	-73
5	65	4	45	5762.2958	4.375×10^{-1}	4.534×10^{-1}	4
4	63	4	45	5762.3559	8.882×10^{-1}	1.126×10^{-1}	-87
3	62	4	45	5762.3565	6.840×10^{-1}	3.378×10^{-1}	-51

^a Our recommended wavenumbers with an estimated overall relative uncertainty less than 0.02 cm^{-1} .

^b Our recommended gf -values with an estimated overall uncertainty of 5%.